

# WHAM Observations of $H\alpha$ Emission from High Velocity Clouds in the M, A, and C Complexes

S. L. Tufte, R. J. Reynolds, & L. M. Haffner  
Astronomy Department, University of Wisconsin – Madison

## ABSTRACT

The first observations of the recently completed Wisconsin H-Alpha Mapper (WHAM) facility include a study of emission lines from high velocity clouds in the M, A, and C complexes, with most of the observations on the M I cloud. We present results including clear detections of  $H\alpha$  emission from all three complexes with intensities ranging from 0.06 to 0.20 R. In every observed direction where there is significant high velocity H I gas seen in 21 cm emission we have found associated ionized hydrogen emitting the  $H\alpha$  line. The velocities of the  $H\alpha$  and the 21 cm emissions are well correlated in every case except one, but the intensities are not correlated. There is some evidence that the ionized gas producing the  $H\alpha$  emission envelopes the 21 cm emitting neutral gas but the  $H\alpha$  “halo”, if present, is not large. If the  $H\alpha$  emission arises from the photoionization of the H I clouds, then the implied incident Lyman continuum flux  $F_{LC}$  at the location of the clouds ranges from 1.3 to  $4.2 \times 10^5$  photons  $\text{cm}^{-2} \text{s}^{-1}$ . If, on the other hand, the ionization is due to a shock arising from the collision of the high-velocity gas with an ambient medium in the halo, then the density of the pre-shocked gas can be constrained. We have also detected the [S II]  $\lambda 6716$  line from the M I cloud and have evidence that the [S II]  $\lambda 6716$  to  $H\alpha$  ratio varies with location on the cloud.

*Subject headings:* Galaxy: halo — ISM: clouds

## 1. Introduction

High velocity clouds (HVCs) were discovered over 30 years ago through the 21 cm line of neutral hydrogen (Muller, Oort, and Raimond 1963). While they have been studied extensively (and almost exclusively) in the 21 cm line since then, the origin and nature of HVCs is still largely unknown. They are observationally defined as gas moving at velocities not explainable by cylindrical galactic rotation (a rule of thumb is  $|v_{lsr}| \geq 90 \text{ km s}^{-1}$ ). In

the northern hemisphere, the vast majority of the HVCs have negative velocities, that is, they are falling toward the Galactic plane. In addition, there exists gas at intermediate velocities (IVCs), also primarily falling toward the plane in the northern hemisphere, which may have a connection with the HVCs (see Kuntz & Danly 1996). Many theories have been proposed to explain the HVCs. One model suggests that they are remnants of the formation of the Milky Way only now being captured by the gravitational field of the Galaxy (Oort 1966, Oort 1970, Wakker 1990). Another suggests that they are the cooled condensate of material vented into the halo as a result of super-bubble breakout (the galactic fountain model, see Shapiro & Field 1976, Bregman 1980). Another proposal (Murai & Fujimoto 1980, Giovanelli 1981) is that the gas was tidally stripped from the Magellanic clouds as they orbit the galaxy. There is convincing evidence that this is the case for a southern complex of high velocity gas known of as the Magellanic Stream, but it is harder to associate the northern HVCs with this origin. For a comprehensive review of HVCs, see Wakker & Van Woerden (1997).

One of the principal limitations to progress in understanding the HVCs is the lack of knowledge of the distances to the emitting gas. The only reliable method of determining distances to HVCs is through absorption line spectroscopy toward bright objects of known distance in the direction of the cloud. This method has now been successfully employed to constrain the distance to the M complex and the A complex. Toward the M complex, Danly et al. (1993) have constrained the height  $z$  above the Galactic plane to 1.5 to 4.4 kpc. Wakker et al. (1996) and van Woerden et al. (1997) have constrained the A cloud to be between 3 and 7 kpc above the plane. This places these HVC complexes in the Galactic halo and thus makes them excellent “test particles” for studying the conditions there. The distance to the C complex is still unknown.

While considerable effort has been expended looking for emission lines from HVCs in the past, there have only been a few detections. A search for  $H\alpha$  by Reynolds (1987) in 6 directions toward HVCs, including two directions toward the M complex, yielded negative results. The upper limits placed on the intensity by this study ranged from 0.2 R to 0.6 R. One rayleigh (R) is  $10^6/4\pi$  photons  $\text{cm}^{-2} \text{s}^{-1} \text{sr}^{-1}$ . Kutyrev and Reynolds (1989) obtained a  $4\sigma$  detection of a very high velocity cloud ( $v_{lsr} = -300 \text{ km s}^{-1}$ ) in Cetus. The  $H\alpha$  brightness in this direction was measured to be  $I_\alpha = 0.08 \text{ R}$ . Münch & Pitz (1989) marginally detected high velocity  $H\alpha$  emission from the M II cloud with  $I_\alpha = 0.15 \text{ R}$  (one of our observation directions is very near theirs, and we compare the results below). Songaila et al. (1989) claim a detection of  $H\alpha$  from high velocity gas in complex C. The intensity they measured was 0.03 R; however, we here present observations of the same direction and find the emission to be significantly brighter than the Songaila & Cowie measurement. Very recently, Weiner & Williams (1996) have detected  $H\alpha$  emission from a number of directions

toward the Magellanic Stream. They find that  $H\alpha$  emission enhancements (typically  $\simeq 0.2$  R) are associated with gradients in the H I distribution, which they interpret as evidence that the emission is produced by ram pressure heating of the cloud as it passes through a low density ambient medium. In general, the previous observations of  $H\alpha$  from HVCs required long integration times and, with the exception of the Magellanic Stream detections, produced null or marginal results.

Much can be learned about both the HVCs and the Galactic halo environment from a study of optical emission lines. For example, the brightness of the  $H\alpha$  line gives information on the amount of ionized hydrogen that is associated with the neutral gas. If the ionizations are due to photoionization, then the  $H\alpha$  intensity is a direct measure of the Lyman continuum flux incident upon the cloud. Measurements of this flux at various locations above the plane of the Galaxy can have an important bearing on more general questions regarding ionized gas in the disk and halo of the Milky Way. If the ionizations are due to collisional processes induced by the rapid motion of the cloud (i.e. shocks), then the intensity is a measure of the ambient density of material through which the cloud travels. It may be possible to distinguish between these two ionization mechanisms by measuring other emission lines such as [O III]  $\lambda 5007$ , [S II]  $\lambda 6716$ , and [N II]  $\lambda 6584$ . It is also possible that the pattern of  $H\alpha$  intensity may shed some light on the relationship between the neutral and ionized gas and perhaps features in the ISM at lower velocity.

## 2. Observations

The Wisconsin H-Alpha Mapper (WHAM) is a recently completed facility that is located at Kitt Peak, AZ and is operated remotely from Madison, WI (Reynolds et al. 1998; Tufte 1997). The WHAM instrument is optimized for the detection and study at high spectral resolution of faint optical emission lines from spatially diffuse astronomical sources. By employing the largest available Fabry-Perot etalons and a state of the art CCD chip as an imaging detector, the WHAM instrument achieves unprecedented sensitivity for velocity resolved studies of faint emission lines from diffuse sources. This opens a new window to the HVCs.

The new WHAM spectrometer is well suited to the study of emission lines from HVCs for several reasons: 1) the Fabry-Perot spectrometer is ideal for detecting spatially extended emission from faint sources at high resolving power due to the much higher throughput available at a given spectral resolution compared to grating spectrometers, 2) the 15 cm etalons used by the WHAM spectrometer are the largest available, 3) the  $1^\circ$  beam is well matched to the large angular sizes characteristic of many of the HVCs, and 4) the 12

km s<sup>-1</sup> resolution is well matched to the 20–25 km s<sup>-1</sup> (FWHM) line widths (21 cm) typical of HVCs. As a result, the WHAM spectrometer allows us to obtain clear detections of emissions with intensity of order 0.1 R in 30 minutes integration time.

We obtained H $\alpha$  observations in 15 directions in the vicinity of the high-velocity clouds M I and M II. Table 1 lists the coordinates of each look direction along with the total exposure time and the date(s) of observation. Figure 1 shows our look directions on a map of 21 cm contours from the Leiden/Dwingeloo survey (Hartmann & Burton 1997). The 21 cm data measure the amount of neutral hydrogen at high velocity ( $v_{lsr} \leq -80$  km s<sup>-1</sup>). The M complex H $\alpha$  study was conceived as a set of 8 “on–off” pairs. The directions 1a, 2a, 5a, 6a, 7a, and 8a are “on” the M I cloud as defined by the 21 cm maps, and the associated “off” directions, which are 4a, 3a, 9a, 12a, 11a, and 10a, were chosen based on their lack of detected H I gas at high velocity. Note that directions 9a and 11a do not appear on this map and that 7a, while near the M I cloud, is not within the the lowest 21 cm column density contour. For the M II cloud, the “on” directions are 1b and 2b, and the “off” direction is 3b (see Fig. 1). The M clouds are especially interesting because of their high Galactic latitude ( $50^\circ \leq b \leq 70^\circ$ ). At this latitude, Galactic rotation cannot be a significant factor in the radial velocity, which is then a fairly good measure of motion perpendicular to the Galactic plane. Further, dust obscuration is less significant than at lower latitudes.

We have also obtained H $\alpha$  observations in 4 directions toward the A complex (2 “on” directions and 2 “off” directions) and 2 directions toward the C complex (1 “on” direction and 1 “off” direction). The locations of these beams for the A complex and the C complex are shown on maps of the 21 cm intensity contours in Figure 2 and Figure 3, respectively. The “off” directions for the C complex are off the map.

We use the “on” minus “off” method in order to isolate the emission due to the HVCs under study. This requires an observation “on” the direction of interest, immediately followed by an observation of a nearby direction that is “off” the high velocity cloud. This very powerful technique allows for the subtraction of the sky spectrum and cancellation of many systematic uncertainties. Since the intermediate velocity gas (IVC) extends over the entire region around complex M and is fairly smooth (at least in the 21 cm maps), this method also serves to subtract off the IVC component, allowing for the isolation of the HVC component. Figure 4 shows an example of the method. The upper panel depicts the spectrum of an “on” direction (derived from a 900 second exposure of the 1a direction) as a solid line and the spectrum of an “off” direction (derived from a 900 second exposure of the 4a direction taken immediately after the 1a exposure) as a dashed line. Both spectra show the relatively bright geocoronal H $\alpha$  emission line on the right and very little else. The geocoronal emission line is placed near the red edge of the bandpass for use in the

velocity calibration. The irregularity near the blue edge of the spectrum is a remnant of the flat-fielding process. The lower panel shows the result of subtracting the “off” spectrum from the “on” spectrum. Here one can clearly see an emission component near  $-110 \text{ km s}^{-1}$  due to the M I cloud. On the right, the difference spectrum takes a steep dive due to a combination of the fact that the geocoronal line is brighter in the “off” direction and that the 4a direction has more emission from lower velocity gas (see below). In general, problems with accurately correcting for the roll off at the edge of the aperture make it difficult to measure extremely faint emission lines at velocities between  $-200 \text{ km s}^{-1}$  and  $-175 \text{ km s}^{-1}$ . Problems with accurately removing the geocoronal line make it difficult to extract information at velocities greater than about  $-40 \text{ km s}^{-1}$ . This leaves a velocity interval of  $130 \text{ km s}^{-1}$  within which we can make good measurements of very faint emissions from high velocity gas.

We discovered several emission lines in the night sky spectrum that are probably extremely weak, not previously detected OH lines. Figure 5 shows the average of two spectra from the February 24 observations. On this night, the sky lines were the brightest, although the same lines are present to some degree in all of the spectra. The evidence for the lines originating in the atmosphere and not the Galaxy is: 1) the lines are present in all of the spectra (both “on” and “off”), 2) their brightness seems to depend more on the night than the look direction, 3) the location of the lines is fixed with respect to the geocoronal line and not fixed with respect to the LSR, and 4) the lines appear to be very narrow, as would be expected for atmospheric lines but not Galactic emission. The night sky features were fitted with Gaussian components at locations shown by the arrows in Figure 5. A terrestrial spectrum was then subtracted from each spectrum as part of the data reduction process. This spectrum was formed using the spectrum shown in Figure 5 as a template. The locations and relative strengths of the sky lines were held fixed and a single parameter corresponding to the overall brightness of the sky lines was adjusted by fitting the brightest line (the second from the left) in each spectrum. The brightest terrestrial line, on the night when the sky line contamination was the worst (1996 February 24), is slightly brighter than the M I cloud (1a–4a) emission. On all other nights, the brightest line is  $\lesssim 1/3$  of the M I cloud intensity. The analysis of the “on–off” pairs was done with and without this night sky line subtraction to insure that the process was not introducing spurious emission features. The results for the “on–off” spectra were very similar in the two cases, as is expected since the sky line intensities change little on hour time scales.

For directions 1a, 4a, 6a, and 12a we also obtained spectra in the [S II]  $\lambda 6716$  line. On 1996 April 10, two 900 second exposures were obtained for each of these directions.

### 3. Results

#### 3.1. The H $\alpha$ “on–off” Spectra

##### 3.1.1. *M Complex*

The spectrum obtained by averaging the 5 “on–off” pairs measured for the 1a–4a direction is shown in Figure 6. An emission line is clearly detected at a velocity with respect to the local standard of rest (LSR)  $v_{lsr} = -106 \pm 1 \text{ km s}^{-1}$ . For  $v_{lsr} \leq -170 \text{ km s}^{-1}$  the spectrum rises due to our current inability to accurately correct for the roll-off caused by vignetting. For  $v_{lsr} \geq -50 \text{ km s}^{-1}$  the spectrum decreases sharply due to differences in the intermediate velocity gas intensity and the geocoronal intensity between the “on” and the “off” directions (i.e., the H $\alpha$  emission associated with the lower velocity gas is brighter in the “off” direction). A Gaussian fit to the emission line, convolved with the instrumental response function, is shown as the solid curve in Figure 6. The extent of the curve shows the velocity range included in the fit. The area under this curve leads to an intensity for this emission line of  $0.078 \pm 0.010 \text{ R}$  and the full width at half maximum (FWHM) is  $27 \pm 4 \text{ km s}^{-1}$ . It must be emphasized that this is the difference between the emission seen in the 1a direction and the 4a direction and that the emission spectrum for the 1a direction alone would be quite different. The intermediate velocity gas (at least the neutral portion) is a fairly uniform sheet in this part of the sky, and so subtracting the 4a direction allows us to extract just the emission due to the the M I cloud. The arrow in the Figure 6 shows the location of the 21 cm emission line from neutral hydrogen derived from the Leiden/Dwingeloo survey. Table 2 summarizes the results from all of the “on–off” pair analysis.

In order to get a handle on the measurement uncertainties, we fitted each of the 5 “on–off” pairs for the 1a–4a direction separately and then compared the scatter obtained in the mean, width, and area parameters of these fits to the uncertainties reported by the fitting program for these parameters. The values are in good agreement, implying that the uncertainties calculated by the fitting program can be used to estimate the uncertainties involved in measuring the parameters of the emission lines. Table 2 lists the calculated uncertainty for each fitted parameter in this and the other HVC H $\alpha$  observation directions. It must be emphasized that these parameters are those of the “on–off” spectrum and that there are potentially significant biases caused by the fact that the “off” spectrum contains some unknown quantity of interstellar H $\alpha$  emission.

The velocities determined for each of the five separate “on–off” 1a–4a pairs have an average value of  $-106.1 \text{ km s}^{-1}$  with  $\sigma_v = 1.0 \text{ km s}^{-1}$ . This small scatter is a strong

confirmation that the emission line is of Galactic origin, since the earth’s motion along the line of sight changed by approximately  $20 \text{ km s}^{-1}$  during the time spanned by the five 1a–4a observations.

Figure 7 shows the 6a–12a difference spectrum. Although the base line is less well-behaved in this case, an emission line is again clearly seen at the same velocity as the 21 cm component. The intensity of this line is  $0.18 \pm 0.02 \text{ R}$ , over twice that found in the 1a direction. This is interesting since the H I column density in the 6a direction is at most 1/6 (and possibly 0.04) times that in the 1a direction. Figure 1 shows that the 1a direction is located near the peak of the 21 cm enhancement while the 6a direction is at the edge of the M I cloud. The implications of this observation are discussed in more depth in Section 4. A more direct comparison of the  $\text{H}\alpha$  intensity from directions 1a and 6a could be made by subtracting the same background direction. This is impossible in this instance because there is no “off” direction that was observed on both the 6a night and one of the 1a nights, and one cannot subtract an “off” direction spectrum taken on a different night because the sky spectrum changes and the “on–off” technique breaks down. However, there is no reason to expect large differences in the high velocity  $\text{H}\alpha$  between the 4a and the 12a directions since neither has detectable 21 cm emission at the velocity of the M I cloud. The available evidence suggests that they are quite similar, making it unlikely that the greater intensity seen in the 6a direction is due to the different “off” directions that were used.

Figure 8a shows the 2a–3a spectrum. The intensity represented by this emission line is  $0.15 \pm 0.02 \text{ R}$ , comparable to the 6a–12a value. The baseline drops sharply on the red edge of the line due to bright intermediate velocity gas in the 3a direction (see below). The velocity of the  $\text{H}\alpha$  emission line is well matched to the 21 cm emission line velocity. Since spectra of the 4a direction were obtained on three of the four observation nights, 4a can be used as a common background direction in many cases to explore possible uncertainties that might be associated with using a different “off” direction in each difference spectrum. Figure 8b shows the 2a–4a spectrum. The 2a spectrum is the average of spectra derived from two 900 second exposures taken on February 24, 1996. On this night we also observed the 4a direction with two 900 second exposures (see Table 1). In general, spectra taken on the same night are close enough in time so that the sky spectrum can be subtracted out effectively. The 2a–4a emission line has an intensity of  $0.20 \text{ R}$ . This is significantly more emission than the 2a–3a line ( $0.15 \text{ R}$ ), and the difference is mainly due to the difference in the fitted widths; the 2a–4a peak height is only slightly greater than the 2a–3a, and the blue side of the two lines look quite similar. This increase in width is a result of there being less  $\text{H}\alpha$  emission from intermediate velocity gas in the 4a direction than in the 3a direction. This comparison demonstrates that the results obtained for the emission lines in “on–off” pair spectra do depend somewhat on the “off” direction due to the fact that the

“off” directions also contain  $H\alpha$  emission, but at generally lower velocities than the HVC detections.

Figure 9a shows the 5a–9a spectrum. This spectrum is fairly noisy, and the baseline is not very well behaved. Nevertheless, there appears to be an emission line at the same velocity as the HVC 21 cm emission. The result of subtracting a 4a spectrum taken on the same night is shown in Figure 9b. The emission line seen in the 5a–4a spectrum is somewhat fainter than the one in the 5a–9a spectrum. The fit shown in Figure 9a gives an intensity of  $0.09 \pm 0.02$  R, while the fit in Figure 9b corresponds to an intensity of  $0.06 \pm 0.02$  R.

Figure 10 shows the the 8a–4a spectrum. This emission line has an intensity of 0.1 R, comparable to the 1a–4a direction. In this case there appears to be a relatively large ( $20 \text{ km s}^{-1}$ ) offset between the  $H\alpha$  and 21 cm components. However, the large difference in widths suggest that there just may be “extra” intermediate velocity  $H\alpha$  emission in 8a relative to 4a, making the  $H\alpha$  line in the difference spectrum appear wider.

The 7a–11a spectrum is displayed in Figure 11a. Because 7a is just off the edge of the main H I cloud and 11a is far ( $\simeq 16$  degrees) from M I, the non-detection of HVC  $H\alpha$  in this spectrum is evidence against a large halo of ionized gas surrounding the neutral M I cloud. The 7a–4a spectrum (Fig. 11b) also shows no high velocity emission component; if anything, there is a dip, possibly due to the presence of a small amount of high velocity gas in the 4a direction.

A few of the  $H\alpha$  observations were devoted to a search for ionized gas in the M II cloud. Figure 12a shows the 2b–3b  $H\alpha$  spectrum, where 2b is near the peak of the M II cloud 21 cm enhancement (see Fig. 1). The  $H\alpha$  spectrum shows a clear emission component that is shifted toward less negative velocities than the M I cloud components. This lower velocity is also apparent in the H I data. Figure 12b shows the result of subtracting the spectrum of the “standard” background direction, 4a, from the 2b spectrum. In this case, the emission was fitted with two Gaussian components, since the component has an obvious non-Gaussian flat-top shape. The component with a more negative velocity in this fit is centered at  $-78 \text{ km s}^{-1}$  and has an intensity of 0.16 R. This velocity is not too far from the 21 cm velocity of  $-86 \text{ km s}^{-1}$  found for the 2b direction. The red component at  $-50 \text{ km s}^{-1}$  is more in the velocity range normally considered “intermediate velocity” gas. Once again, because of the difficulties in isolating the emission components it is not clear whether there is a real difference between the  $H\alpha$  and 21 cm velocities. Also, it is interesting to note that our results are in good agreement with the lower signal to noise Münch and Pitz (1989) detection of  $H\alpha$  emission in a sightline ( $l = 185.0^\circ$ ,  $b = 65.0^\circ$ ) very near 2b. They measured a component at  $v_{lsr} = -80 \text{ km s}^{-1}$  with  $I_\alpha = 0.15$  R. The 1b–4a  $H\alpha$  spectrum is shown



in Figure 13. There is a clear emission component but it is at relatively low velocity ( $-61 \text{ km s}^{-1}$ ), consistent with the lower negative velocity of the 2b direction.

### 3.1.2. A Complex

Figure 14a shows the  $\text{H}\alpha$  spectrum for the A III cloud observation ( $l = 148.5^\circ$ ,  $b = 34.5^\circ$ ) resulting from the average of four 900 second exposures “on” the direction minus the average of four “off” observations. Notice that the spectrometer was “tuned” to cover a higher negative velocity interval than for the M complex observations. This is accomplished by changing the optical path length in the Fabry-Perot etalon gaps by changing the gas pressure in the etalon chambers. The spectrum shows a clear detection of an emission line at a velocity of  $v_{lsr} = -167 \pm 1 \text{ km s}^{-1}$ . The arrow in the figure shows the velocity of the component detected for the 21 cm line in the Leiden/Dwingeloo survey data, which appears to have a significant offset from the  $\text{H}\alpha$  velocity. The  $\text{H}\alpha$  intensity derived from the fit shown in Figure 14a is  $I_\alpha = 0.08 \pm 0.01 \text{ R}$ .

Figure 14b shows the  $\text{H}\alpha$  spectrum measured for the A IV cloud direction ( $l = 153.6^\circ$ ,  $b = 38.2^\circ$ ), the average of four 900 second “on” exposures minus the average of three 900 second “off” exposures. The emission feature detected in this case has an intensity of  $I_\alpha = 0.09 \pm 0.01 \text{ R}$  and a velocity of  $v_{lsr} = -178 \pm 1 \text{ km s}^{-1}$ . The arrow in the figure shows the velocity of the 21 cm emission, which does match the  $\text{H}\alpha$  component velocity.

### 3.1.3. C Complex

Figure 15 shows the  $\text{H}\alpha$  difference spectrum for the C complex direction ( $l = 84.3^\circ$ ,  $b = 43.7^\circ$ ). While the baseline is not well determined, an emission component is clearly detected at a velocity matching that of the 21 cm component. The  $\text{H}\alpha$  intensity of this component is  $I_\alpha = 0.13 \pm 0.03 \text{ R}$ , and the velocity is  $v_{lsr} = -111 \pm 2 \text{ km s}^{-1}$ . Songaila, Bryant, & Cowie (1989) observed this same look direction (their Position 1, see their Fig. 1a). They report a detection with an intensity of 0.03 R and an estimated uncertainty of 50%. Our higher signal to noise observation is inconsistent with this result.

## 3.2. The [S II] $\lambda 6716$ “on–off” Spectra

Figure 16a shows the [S II]  $\lambda 6716$  spectrum of the 1a–4a direction in the M I cloud. The spectrum strongly suggests the presence of [S II] emission at a velocity very close to

the velocity at which H $\alpha$  emission was detected in this direction (indicated by an arrow in the figure). The best fit intensity is  $0.05 \pm 0.01$  R, and the width is  $23 \pm 8$  km s $^{-1}$  (the uncertainties quoted here are the formal errors calculated in the fitting process). The mean velocity is  $v_{lsr} = -110 \pm 3$  km s $^{-1}$ . The spectrum also suggests another smaller peak near  $-60$  km s $^{-1}$  (not fitted). Figure 16b shows the [S II]  $\lambda 6716$  spectrum of the 6a–12a direction. This spectrum does not show a clear [S II] detection; however, there is a marginal enhancement at  $-96$  km s $^{-1}$ . The Gaussian fit to this enhancement corresponds to an intensity of  $0.02 \pm 0.01$  R and a width of  $18$  km s $^{-1}$ . We will treat the fitted intensity as an upper limit to the [S II] emission from this direction. The [S II] / H $\alpha$  ratios for the two directions are then:

$$\left(\frac{I_{\text{S II}}}{I_{\text{H}\alpha}}\right)_{1a4a} \simeq 0.64 \pm 0.14, \quad (1)$$

and

$$\left(\frac{I_{\text{S II}}}{I_{\text{H}\alpha}}\right)_{6a12a} \lesssim 0.11 \pm 0.06, \quad (2)$$

a difference of a factor of six. This large difference in the [S II] / H $\alpha$  ratio indicates significant variations in ionization/excitation conditions within the M I cloud.

#### 4. Discussion and Conclusions

We have searched for H $\alpha$  emission from five high velocity clouds in three cloud complexes. In every direction where there is significant high velocity H I gas seen in 21 cm emission, an associated H $\alpha$  line was detected. Also, except for 6a, which is just off the edge of the M I cloud, there is no clear evidence of H $\alpha$  in any of the directions without appreciable H I emission. Nevertheless, while there is a close correspondence between high velocity 21 cm and H $\alpha$  emission on the sky, the intensities of the 21 cm and H $\alpha$  are not well correlated. Figure 17 shows the H $\alpha$  intensity in Rayleighs from Table 2 plotted versus the 21 cm column density determined from the Leiden/Dwingeloo data for the M complex directions. No correlation is apparent in the plot. The brightness of the 6a direction provides some evidence that the ionized gas producing the H $\alpha$  emission envelopes the 21 cm emitting neutral gas. However, the H $\alpha$  “halo”, if present, is not large, as is shown, for example, by the nondetection of H $\alpha$  in the 7a direction. A complete map of the high velocity H $\alpha$  emission in this region would be very illuminating in this regard.

On the other hand, the velocities of the components found in the H $\alpha$  spectra do correlate with the velocities found in the 21 cm data. Figure 18 shows a plot of the H $\alpha$  component velocities versus the 21 cm component velocities. A good correlation between the two exists, indicating that the H $\alpha$  emission is clearly associated with the H I clouds

seen in the 21 cm line. The scatter is consistent with our current measurement errors. The systematic offset (of  $-10 \text{ km s}^{-1}$ ) of the  $\text{H}\alpha$  from the 21 cm is tantalizing, but may well also be due to biases introduced by the “on–off” subtraction method (see below).

The widths of the  $\text{H}\alpha$  components are very uncertain. This is due to the fact that in many cases the high velocity emission is blended with intermediate velocity emission, which the “on–off” method subtracts out, but not without introducing biases into the measured line widths (and therefore also positions) of the high velocity emission component. The 1a–4a direction provides the best measurement we have of a high velocity emission component, and in this direction we measure the width to be  $27 \pm 4 \text{ km s}^{-1}$ . This is quite similar to the  $24 \text{ km s}^{-1}$  line width measured for the 21 cm emission component in this direction (see Table 2). The bias due to the “off” subtraction can be seen by comparing the width found for the 2a–3a spectrum ( $W = 38 \text{ km s}^{-1}$ ) to that measured for the 2a–4a spectrum ( $W = 49 \text{ km s}^{-1}$ ). As another example, the 5a–9a emission line has a width of  $46 \text{ km s}^{-1}$ , while the 5a–4a emission line is  $38 \text{ km s}^{-1}$  wide. Therefore, the component widths are not determined well, and the width uncertainties listed in Table 2, which were calculated from the quality of the fits and without considering the bias due to the “off” subtraction, are underestimated. The [S II] line width in the 1a direction appears to be narrower than the  $\text{H}\alpha$  line width, but is highly uncertain. The formal fit gives  $23 \pm 8 \text{ km s}^{-1}$  (FWHM) for the [S II] line width compared to  $27 \pm 4 \text{ km s}^{-1}$  for the  $\text{H}\alpha$  line.

Jura (1979) has suggested the possibility of detecting high velocity  $\text{H}\alpha$  emission that originates in the plane of the Galaxy and is reflected off of dust contained in HVCs. This emission would have radial velocities approximately twice that of the 21 cm emission and hence, this is not the origin of the the emission line detections reported here. The velocities expected for this reflected emission are unfortunately outside the range probed in this study. However, a search for it in a future study is a viable and interesting possibility that could provide unique information on the optical transparency of the Galactic disk as well as further measurements of the dust content of the HVCs.

Since interstellar extinction can be neglected along these high latitude sightlines (especially for the M complex observations), the  $\text{H}\alpha$  intensity towards a high-velocity cloud is directly related to the emission measure ( $\text{EM} \equiv \int n_e^2 dl$ ) through the cloud and gives information on the column density of ionized hydrogen and the electron density associated with the cloud. As an example, consider the 21 cm enhancement centered near direction 1a in the M complex. It has an H I column density of  $\simeq 1.5 \times 10^{20} \text{ cm}^{-2}$  (the highest contour level in Fig. 1) and a diameter of about  $1.5^\circ$ , which corresponds to 50 pc at a distance of 2 kpc. Hence the density of neutral hydrogen  $n_{\text{H I}} \simeq 1.0 \text{ cm}^{-3}$ , and the mass of the cloud is about  $1600 M_\odot$ . For direction 1a, we measured  $I_\alpha$  to be approximately 0.08 R, implying an

emission measure  $EM = 0.18 \text{ cm}^{-6} \text{ pc}$ , assuming a temperature for the H II of 8000 K. This leads to an electron density  $n_e \simeq 0.06 f^{-1/2} \text{ cm}^{-3}$  and a column density of ionized hydrogen  $N_{\text{H II}} \simeq 1 \times 10^{19} f^{1/2} \text{ cm}^{-2}$ , where  $f$  is the filling fraction of the H II within the cloud. The H I column density in the 1a direction is  $N_{\text{HI}} \simeq 1.22 \times 10^{20} \text{ cm}^{-2}$ . Since  $f \leq 1$  and there is little evidence that the H II associated with the cloud extends significantly beyond the H I portion of the cloud, this would suggest that at this location the HVC is primarily neutral with  $N_{\text{HII}} / N_{\text{HI}} \lesssim 0.08$ . Interestingly, most of the H II may be located near the outer surface of the cloud. For example, if we consider direction 6a which appears to intersect the edge of the cloud (see Fig. 1), the H I column density is less than  $2 \times 10^{19} \text{ cm}^{-2}$ , whereas the  $\text{H}\alpha$  is twice the intensity of 1a, indicating that there may be as much or more H II as H I along the edge of the H I enhancement.

If the  $\text{H}\alpha$  emission arises from the photoionization of the cloud, then the intensity of the emission is directly related to the incident Lyman continuum flux  $F_{LC}$ . Since the H I cloud is optically thick in the Lyman continuum and optically thin to  $\text{H}\alpha$  photons, each Lyman continuum photon incident on the cloud will ionize a hydrogen atom and each hydrogen recombination will produce on the average 0.46  $\text{H}\alpha$  photons (Martin 1988; Pengally 1964; case B,  $T \sim 10^4 \text{ K}$ ). This leads to the relation

$$F_{LC} = 2.1 \times 10^5 \left( \frac{I_\alpha}{0.1R} \right) \text{ photons cm}^{-2}\text{s}^{-1}.$$

If, on the other hand, the ionization is due to a shock arising from the collision of the high-velocity gas with an ambient medium in the halo,  $I_\alpha$  provides information on the density and temperature of this ambient medium. A cloud velocity of  $100 \text{ km s}^{-1}$  is supersonic for ambient temperatures  $T \leq 10^6 \text{ K}$ . If the ambient gas is sufficiently cool for strong shocks to occur, then we can use shock models by Raymond (1979), which apply to shocks with  $50 \leq V_s \leq 140 \text{ km s}^{-1}$  and relate the face-on  $\text{H}\alpha$  surface brightness  $(I_\alpha)_\perp$  to the halo gas parameters. Namely,

$$(I_\alpha)_\perp \simeq 6.5 n_o \left( \frac{V_s}{100} \right)^{1.7} R,$$

where  $n_o$  is the density of the preshocked gas. This power law is a fit to the predicted  $\text{H}\alpha$  intensities for shock velocities between  $50 \text{ km s}^{-1}$  and  $140 \text{ km s}^{-1}$  presented in Raymond (1979). Hence, for  $V_s = 100 \text{ km s}^{-1}$ , and  $(I_\alpha)_\perp = 0.1 R$  as is the case for the M I cloud, then  $n_o \leq 0.015 \text{ cm}^{-3}$ . This is an upper limit on  $n_o$  because a nonperpendicular sightline will increase the observed  $I_\alpha$  for a given  $n_o$  and  $V_s$ .

The fact that the intensities all seem to be around  $0.1 R$  may be a clue to the ionization mechanism puzzle. This fact is more easily explained in a photoionization scenario in that the various clouds we measure give independent measurements of the same quantity, that

is, the ionizing flux in the Galactic halo (see Bland-Hawthorn & Maloney 1998). It is difficult to explain the uniformity of the  $H\alpha$  intensities in a shock excitation scenario, since in that case the expected  $H\alpha$  flux varies strongly with both the shock velocity and the ambient density. Another weak piece of evidence for photoionization comes from the fairly narrow, albeit poorly measured,  $H\alpha$  line widths, which are similar to the widths observed in photoionized H II regions surrounding O stars (Reynolds 1988). A more careful map of  $I_\alpha$  around the edge of the clouds could also be used to distinguish between the two ionization mechanisms.

If indeed the detected  $H\alpha$  emission results from photoionized gas, then such measurements can shed light on more general questions concerning the interstellar medium in the Galactic halo and its connection to processes occurring in the disk. For example, consider the long-standing problem of the ionization of the Warm Ionized Medium (WIM), an extensive, thick ( $\simeq 2$  kpc) layer of ionized hydrogen in our Galaxy. It has frequently been proposed that the source of the ionization in the WIM is O stars in the plane of the Galaxy (e.g. Domgörgen & Mathis 1994), although other, more exotic sources have also been proposed (e.g. Melott et al. 1988; Sciama 1990). In order to make the O star idea work, very special arrangements of the H I gas must exist to allow photons to get from the Galactic plane, where the vast majority of O stars are located, to gas high above the plane in the thick WIM layer (for specific models that have been constructed to explore this scenario in detail, see Miller & Cox 1993 and Dove & Shull 1994). However, if the H I gas is arranged to be very porous to Lyman Continuum photons, then one would expect a significant fraction of the photons to leak out of the disk and into the halo. The  $H\alpha$  intensity towards H I clouds in the Galactic halo constrains the degree to which this is occurring, and in particular, the  $H\alpha$  intensity towards H I clouds at various distances from the Galactic plane can reveal the Lyman continuum flux as a function of height above the plane. This idea and its implications have been explored from a theoretical stand point by Bland-Hawthorn & Maloney (1998). The  $H\alpha$  intensities we measure for the HVCs are about a factor of 10 lower than typical intensities from WIM gas at high Galactic latitudes, implying that if the ionizing photons originate near the Galactic midplane, 90% of the photons reaching the WIM are absorbed before reaching the heights of the HVCs in the Galactic halo. Note that our measured  $H\alpha$  intensity is an order of magnitude (or more) above what would be expected from the estimated metagalactic ionizing field flux (Ferrera & Field 1994).

Perhaps the question of the source of ionization can be further explored in the future by measuring various emission line ratios. Models by Raymond (1979) predict optical line ratios for shocks under various conditions. With an ambient density  $n_o = 1 \text{ cm}^{-3}$  and a shock velocity  $V_s = 100 \text{ km s}^{-1}$ , some of the predicted line ratios are  $[S \text{ II}] \lambda 6716 / H\alpha =$

0.18,  $[\text{N II}] \lambda 6584 + \lambda 6548 / \text{H}\alpha = 0.51$ , and  $[\text{O III}] \lambda 5007 + \lambda 4959 / \text{H}\alpha = 1.9$ . If this model, when extended to lower densities, retains the prediction of very bright  $[\text{O III}]$  emission, then the  $\lambda 5007$  line could be an important discriminator between shock ionization and photoionization. Note that these emission lines can also give further information on the metal abundances in the HVCs, which have been previously investigated by Lu et al. 1994 and Lu et al. 1998, through absorption line techniques.

It should be noted that the physical conditions in the Galactic halo may vary greatly from location to location. For example, the absorption line measurements of highly ionized halo gas towards Markarian 509 (Sembach et al. 1995, Sembach et al. 1998) suggest a hot ( $\sim 10^5$  K) halo around this HVC. Also, an analysis of Rosat observations of soft X-rays combined with 21 cm data from the new Leiden/Dwingeloo survey toward complex M by Herbstmeier et al. (1995) suggests that there is a brightening of soft X-rays at several cloud locations, perhaps due to collisions of the clouds with the ambient medium in the halo. The most striking such enhancement occurs on the edge of cloud M I, where the H I contours are also seen to be crowded. It should be noted, however, that considerable modeling is necessary to separate out the soft X-rays possibly associated with the M complex region from sources of soft X-rays at other distances in the same direction. The pattern of  $\text{H}\alpha$  intensities, tracing the  $10^4$  K ionized gas, does not seem to correlate well with the soft X-ray brightness derived by Herbstmeier et al. (1995). They calculate that there is an enhancement in soft X-rays emitted by the M I cloud in direction 1a. We do not see enhanced  $\text{H}\alpha$  in this direction. Direction 5a, with no strong X-ray enhancement on the Herbstmeier et al. map, has both comparable 21 cm emission and comparable  $\text{H}\alpha$  emission (see Table 2). On the M II cloud, the 1b direction is at the location of another of the Herbstmeier et al. soft X-ray enhancements, and the 2b direction is located where the soft X-ray emission is thought to be faint. We, on the other hand, find the 2b direction to be significantly brighter in  $\text{H}\alpha$  than the 1b direction.

Finally, improvements in the observational technique may help to eliminate possible systematic errors in line widths and velocities. For example, it is clear from the results in Section 3 that it would be extremely valuable to find an “off” direction with zero Galactic  $\text{H}\alpha$  emission at all velocities. This would allow one to subtract the sky spectrum and correct for other systematic uncertainties without introducing the uncertainty caused by an unknown quantity of emission from the “off” direction. The Lockman Window direction (our 10a) appears to be a good approximation to this ideal. This direction has a famously low H I column density ( $N_{\text{HI}} = 4.4 \pm 0.5 \times 10^{19} \text{ cm}^{-2}$ ; Jahoda, Lockman, & McCammon 1990), and as a result is often used by X-ray astronomers and others interested in looking at sources unobscured by the affects of neutral hydrogen and the associated dust. It also appears to be fainter in  $\text{H}\alpha$  than any other direction we have observed, with  $\text{H}\alpha$

components no brighter than 0.1 R. We are at present carefully examining the spectrum in this direction to determine its usefulness as a “zero emission” standard. We will eventually be able either to detect  $H\alpha$  or put very low upper limits on its intensity by using the shifts in velocity caused by the earth’s orbital motion to distinguish between any actual emission and baseline irregularities or night sky features. If this direction can be used in this way it will not only improve  $H\alpha$  studies of the HVC complexes, but also will allow the study of IVCs in  $H\alpha$ .

We thank Nicole Hausen for her work on the weak atmospheric lines. This work was supported by the National Science Foundation through grants AST 9122701 and AST 9619424.

## REFERENCES

- Bland-Hawthorn, J. & Maloney, P. R. 1998, ApJ, submitted
- Bregman, J. N. 1980, ApJ, 236, 577
- Domgörgen, H., & Mathis, J. S. 1994, ApJ, 428, 647
- Danly, L., Albert, C. E., & Kuntz, K. D., 1993, ApJ, 416, L29
- Dove, J. B., & Shull, J. M. 1994, ApJ, 430, 222
- Ferrara, A., & Field, G. B. 1994, ApJ, 423, 665
- Giovanelli, R. 1981, AJ, 86, 1468
- Hartmann, D. & Burton, W. B. 1997, Atlas of Galactic Neutral Hydrogen, Cambridge University Press
- Herbstmeier, U., Mebold, U., Snowden, S. L., Hartmann, D., Burton, W. B., Moritz, P., Kalberla, P. M. W., & Egger, R. 1995, Astron. Astrophys., 298, 606
- Jahoda, K., Lockman, F. J., & McCammon, D. 1990, ApJ, 354, 184
- Jura, M. 1979, ApJ, 227, 798
- Kuntz, K. D., & Danly, L. 1996, ApJ, 457, 703
- Kutyrev, A. S., Reynolds, R. J., 1989, ApJ, 334, L9
- Lu, L., Savage, B. D., & Sembach, K. R. 1994, ApJ, 426, 563
- Lu, L., Savage, B. D., Sembach, K. R., Wakker, B. P., Sargent, W. L. W., & Oosterloo, T. A. 1998, ApJ, 115, 162
- Martin, P. C. 1988, Ap. J. Suppl., 66, 125
- Melott, A. W., McKay, D. W., & Ralston, J. P. 1988, ApJ, 324, L43
- Miller, W. W. III, & Cox, D. P. 1993, ApJ, 417, 579
- Muller, C. A., Oort, J. H., & Raimond, E. 1963, C. R. Acad. Sci., Paris, 257, 1661
- Münch, G., Pitz, E., 1989, H $\alpha$ -emission in directions toward high-velocity 21-cm clouds, in Tenorio-Tagle, G., Moles, M., Melnich, J. (eds.), Structure and Dynamics of the Interstellar Medium, Proc. IAU Coll. 120, Springer-Verlag, Berlin, Heidelberg, New York, Lecture Notes in Physics, Vol. 350, p. 373
- Murai, T., & Fujimoto, M. 1980, Publ. Astron. Soc. Japan, 32, 581
- Oort, J. H. 1966, Bull. Astr. Inst. Neth., 18, 421
- Oort, J. H. 1970, Astron. Astrophys., 7, 381



- Pengally, R. M. 1964, M.N.R.A.S., 127, 145
- Raymond, J. C. 1979, Ap. J. Suppl., 39, 1
- Reynolds, R. J. 1987, ApJ, 323, 553
- Reynolds, R. J. 1988, ApJ, 333, 341
- Reynolds, R. J., Tufte, S. L., Haffner, L. M., Jaehnig, K., & Percival, J. W. 1998, PASA, 15
- Sciama, D. W. 1990, ApJ, 364, 549
- Sembach, K. R., Savage, B. D., Lu, L., & Murphy, E. M. 1995, 451, 616
- Sembach, K. R., Savage, B. D., Lu, L., & Murphy, E. M. 1998, in preparation.
- Shapiro, P. R., & Field, G. 1976, ApJ, 205, 762
- Songaila, A., Bryant, W., & Cowie, L. L., 1989, ApJ, 345, L71
- Tufte, S. L. 1997, PhD Thesis, University of Wisconsin–Madison.
- van Woerden, H., Wakker, B. P., Schwarz, U. J., Peletier, R. F., & Kalberla, P. M. W. 1997, in IAU Colloq. 166, The Local Bubble, ed. D. Breitschwerdt & M. Freiberg, Springer Lecture Notes in Physics.
- Wakker, B. P. 1990, PhD. thesis, Univ. Groningen
- Wakker, B. P., Howk, C., Schwarz, U. J., van Woerden, H., Beers, T. C., Wilhelm, R., Kalberla, P. M. W., & Danly, L. 1996, 473, 834
- Wakker, B. P., & van Woerden 1997, ARA&A, 35, 217
- Weiner, B. J., & Williams, T. B., 1996, AJ, 111, 1156

Table 1. M Complex H $\alpha$  Observation Data.

Name	$l$ ( $^{\circ}$ )	$b$ ( $^{\circ}$ )	Exp. Time (seconds)	Obs. Date <sup>a</sup>
1a	168.30	65.20	4500	1,2,3
2a	163.30	66.70	1800	2
5a	165.80	65.95	900	3
6a	170.85	64.72	900	4
7a	168.30	67.82	900	3
8a	163.30	64.70	900	3
1b	183.40	65.75	900	2
2b	186.00	65.00	900	2
4a	168.00	70.93	4500	1,2,3
3a	168.30	69.00	1800	2
9a	167.00	60.00	900	3
12a	169.00	74.00	900	4
11a	140.00	80.00	900	3
10a	150.48	52.96	900	3
3b	186.0	70.00	900	2

<sup>a</sup>Observations were carried out on 4 nights,  
1: 2/18/96, 2: 2/24/96, 3: 3/23/96, 4: 4/10/96.

Table 2.  $H\alpha$  and 21 cm Emission from HVCs

Name	$H\alpha$			21 cm		
	$I_{H\alpha}$ (R)	$V_{H\alpha}$ (km s <sup>-1</sup> )	$W_{H\alpha}$ (km s <sup>-1</sup> )	$I_{21cm}$ (10 <sup>20</sup> cm <sup>-2</sup> )	$V_{21cm}$ (km s <sup>-1</sup> )	$W_{21cm}$ (km s <sup>-1</sup> )
M I cloud						
1a-4a	0.08 ± 0.01	-106 ± 1	27 ± 4	1.22	-113	24
2a-3a	0.15 ± 0.02	-98 ± 1	38 ± 3	1.12	-102	40
2a-4a	0.20 ± 0.02	-95 ± 1	49 ± 4	1.17	-101	43
5a-9a	0.09 ± 0.02	-109 ± 2	46 ± 8	1.08	-116	31
5a-4a	0.06 ± 0.02	-103 ± 3	38 ± 10	1.04	-116	30
6a-12a	0.18 ± 0.02	-105 ± 1	35 ± 4	...	...	...
8a-4a	0.11 ± 0.02	-92 ± 2	50 ± 7	0.35	-112	26
M II cloud						
1b-4a	0.12 ± 0.01	-61 ± 2	44 ± 5	1.33	-72	22
2b-3b	0.20 ± 0.02	-72 ± 1	44 ± 4	1.49	-80	26
2b-4a	0.16 ± 0.03	-78 ± 2	27 ± 5	1.50	-80	25
A cloud						
A III	0.08 ± 0.01	-167 ± 1	24 ± 2	1.40	-153	25
A IV	0.09 ± 0.01	-178 ± 1	34 ± 3	1.34	-177	23
C cloud						
C	0.13 ± 0.03	-111 ± 2	38 ± 7	0.54	-120	15

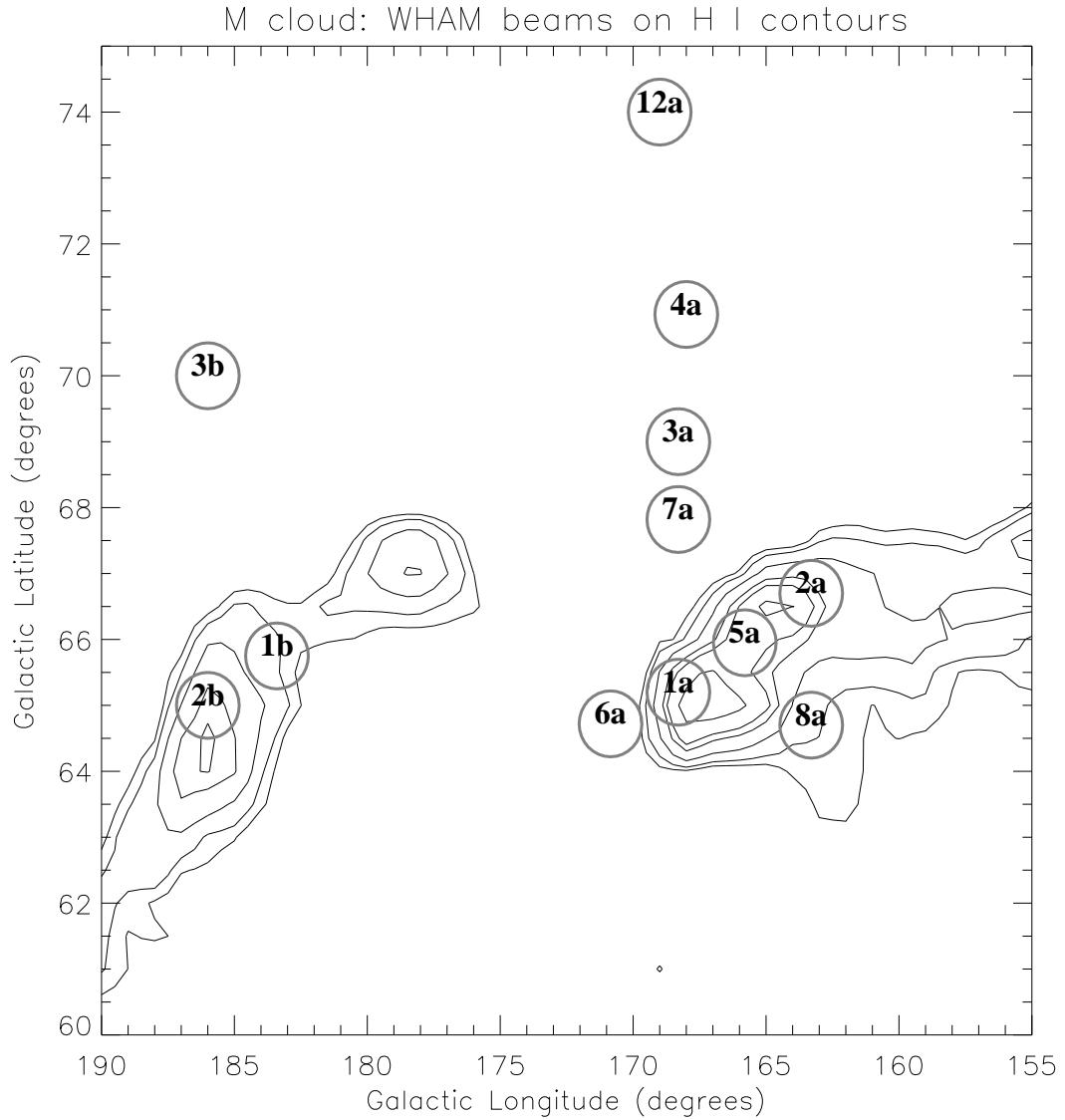


Fig. 1.— WHAM observation directions for the M cloud superposed on 21 cm contours. The 21 cm intensity contours correspond to  $v_{lsr} < -80 \text{ km s}^{-1}$ . The contour levels correspond to  $N_{\text{HI}} = 2.0, 3.0, 5.0, 8.0, 10.0, \text{ and } 15.0 \times 10^{19} \text{ cm}^{-2}$ .

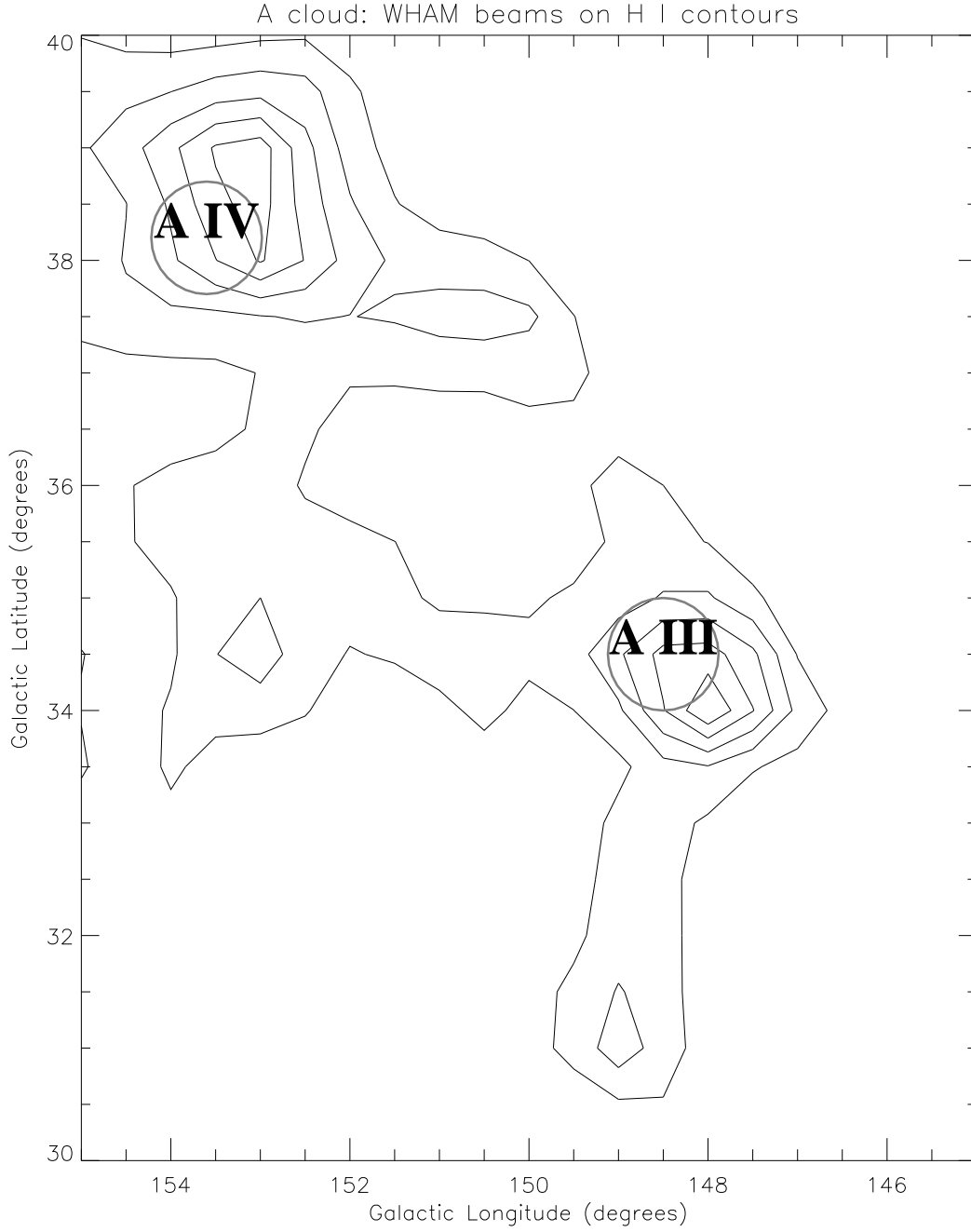


Fig. 2.— WHAM observation directions for the A cloud superposed on 21 cm contours (for  $v_{lsr} < -100 \text{ km s}^{-1}$ ).

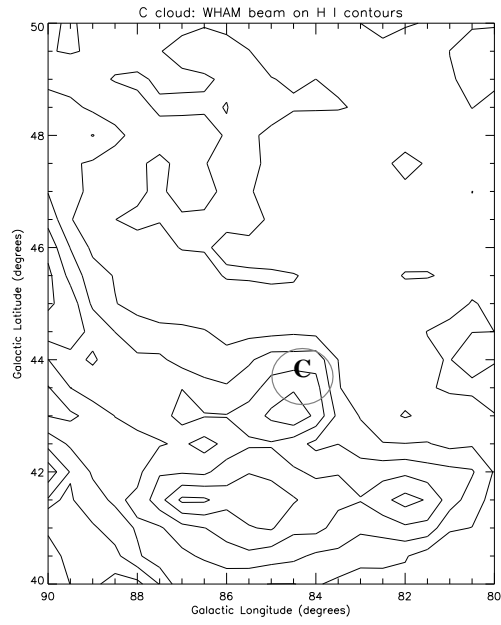


Fig. 3.— WHAM observation direction for the C cloud superposed on 21 cm contours (for  $v_{lsr} < -100 \text{ km s}^{-1}$ ).

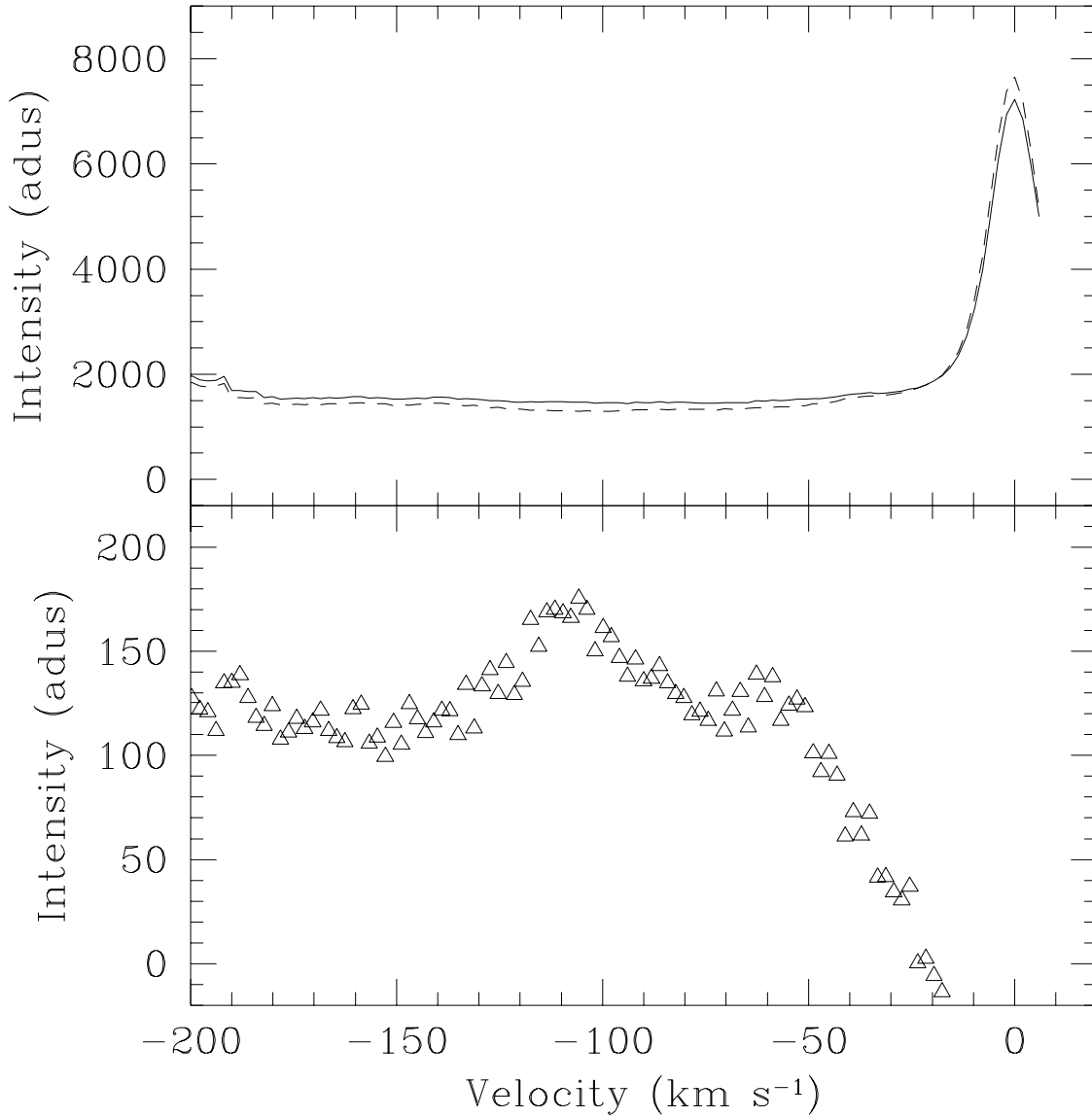


Fig. 4.— H $\alpha$  from the M I cloud: the upper panel shows the spectra derived from single 900 second exposures “on” (the solid line is direction 1a) and “off” (dashed line is direction 4a) the M I cloud. The lower panel shows the difference (“on - off”) spectrum. Note that the units on the intensity axis are arbitrary (adus = “arbitrary data units”).

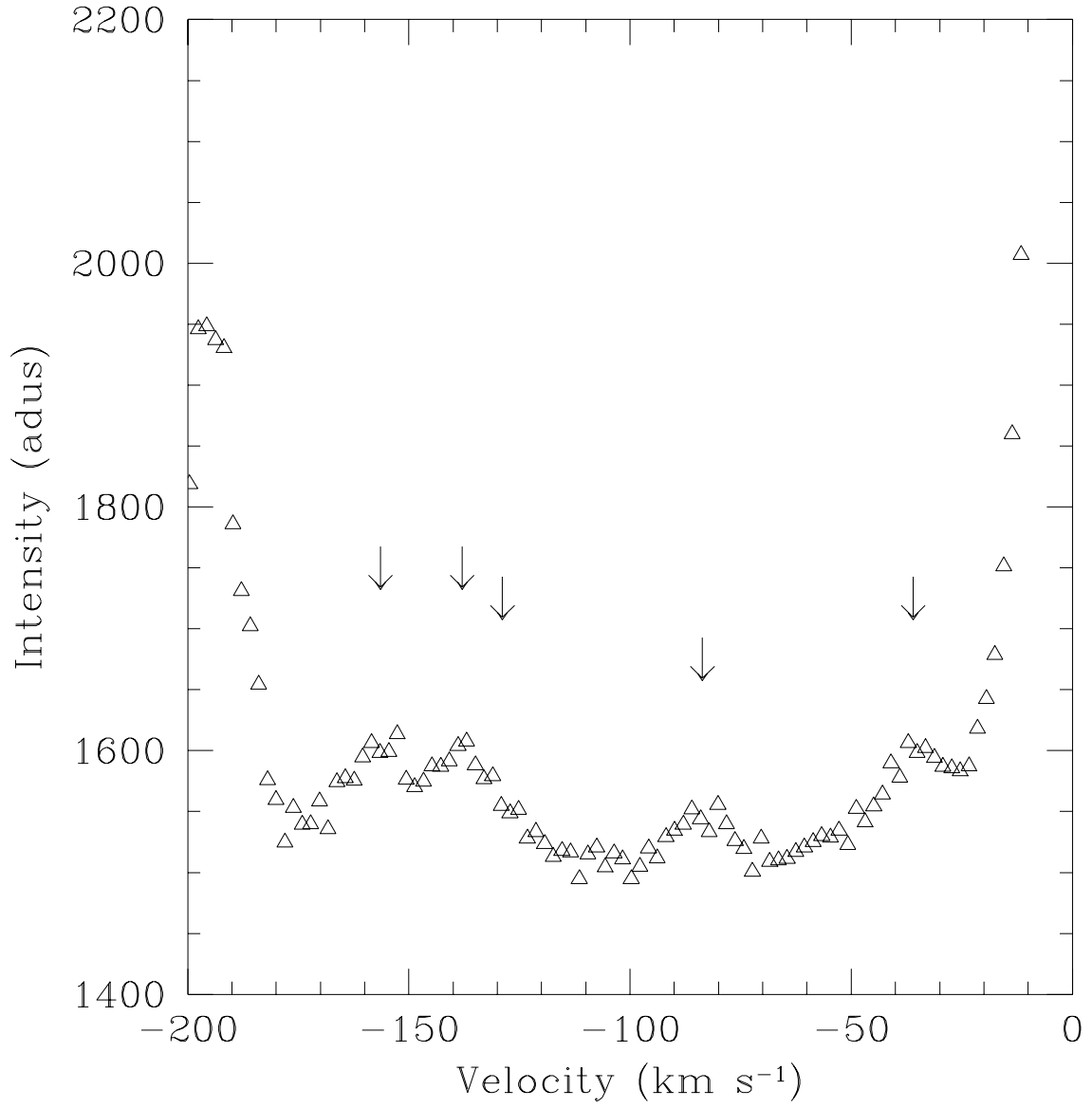


Fig. 5.— Night sky spectral features that are present with variable strength in all the HVC spectra.



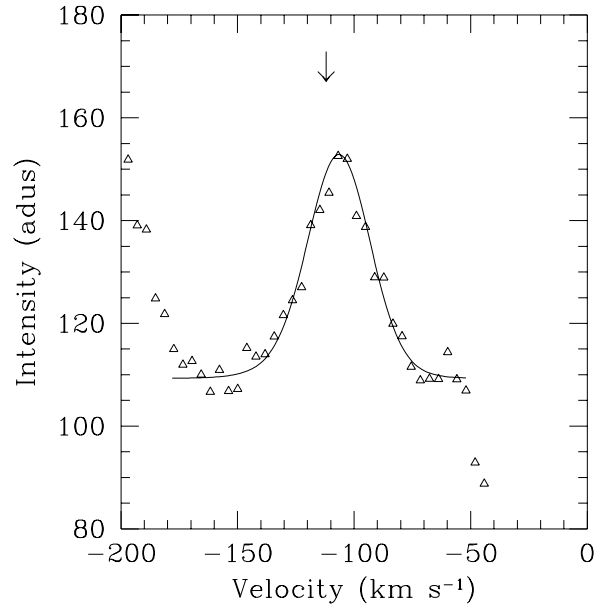


Fig. 6.— H $\alpha$  from the M I cloud: 1a - 4a (normalized to 900s exposure time). The arrow shows the velocity of the 21 cm HVC detection.

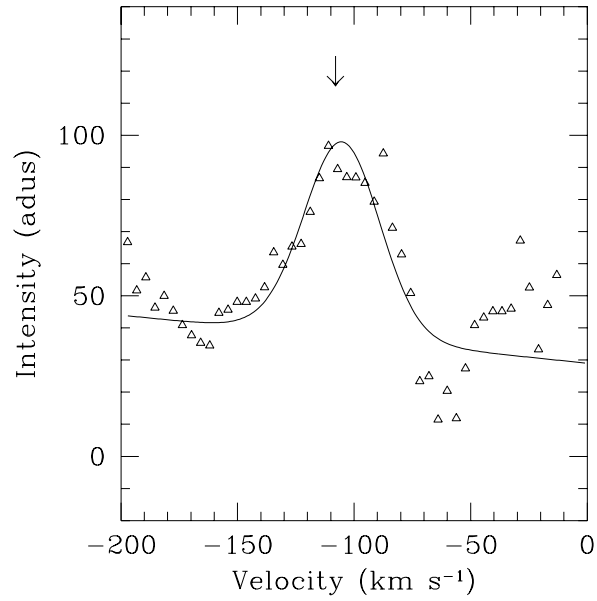


Fig. 7.— H $\alpha$  from the M I cloud: 6a - 12a (900s exposure). The arrow shows the velocity of the 21 cm HVC detection.

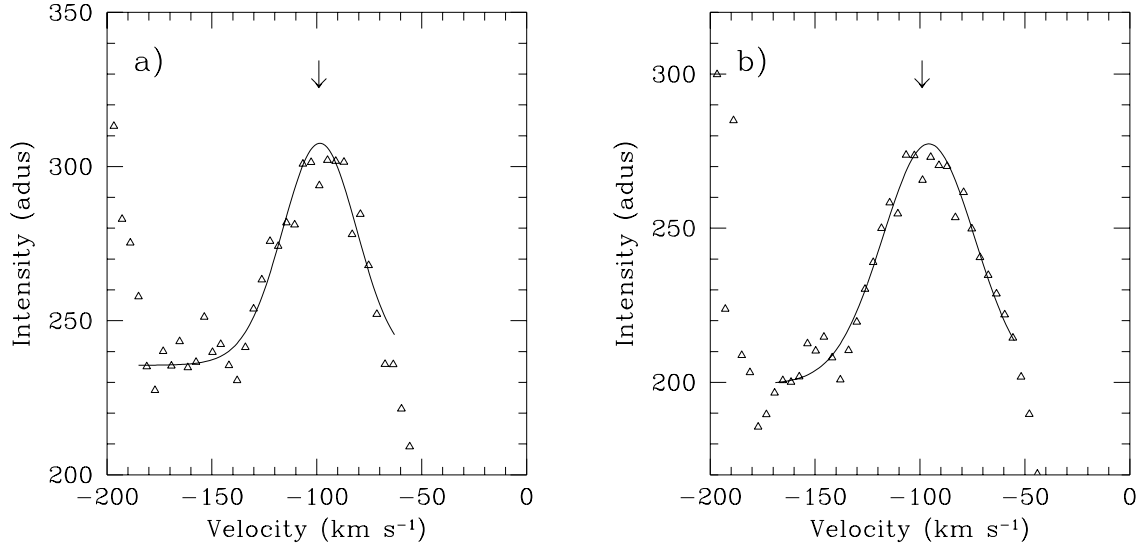


Fig. 8.— H $\alpha$  from the M I cloud: a) 2a - 3a. b) 2a - 4a (both normalized to 900s exposure). The arrows show the velocity of the 21 cm HVC detections.

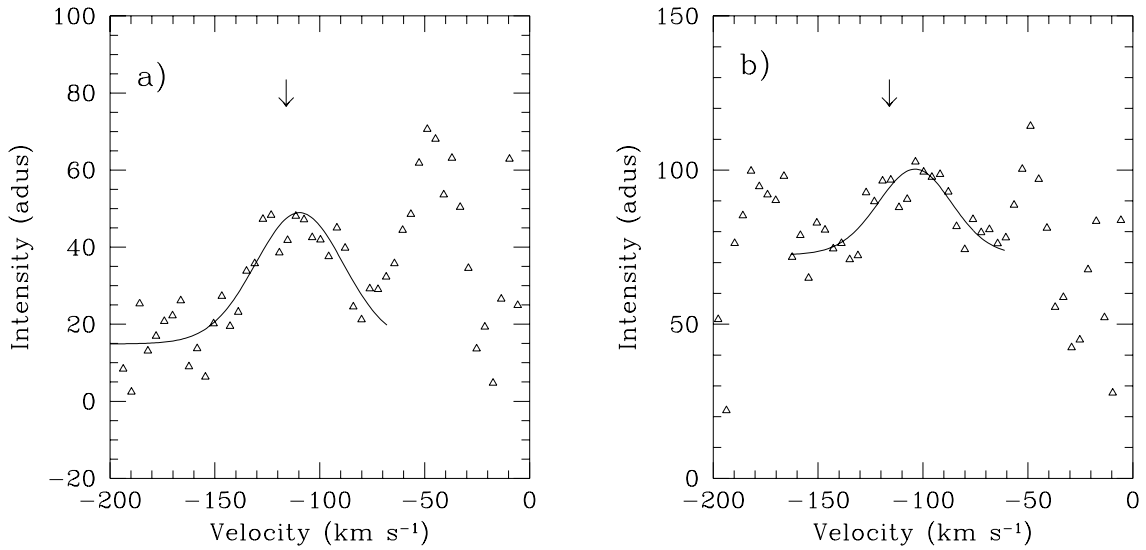


Fig. 9.— H $\alpha$  from the M I cloud: a) 5a - 9a. b) 5a - 4a (both are 900s exposures). The arrows show the velocity of the 21 cm HVC detections.

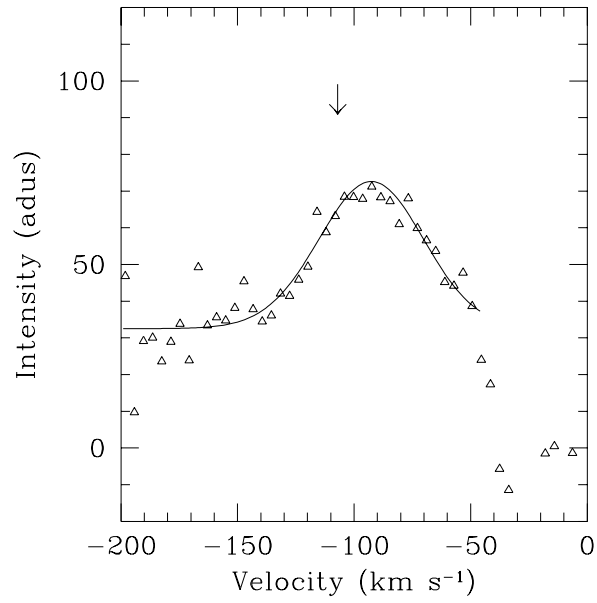


Fig. 10.— H $\alpha$  from the M I cloud: 8a - 4a (900s exposure). The arrow show the velocity of the 21 cm HVC detection.

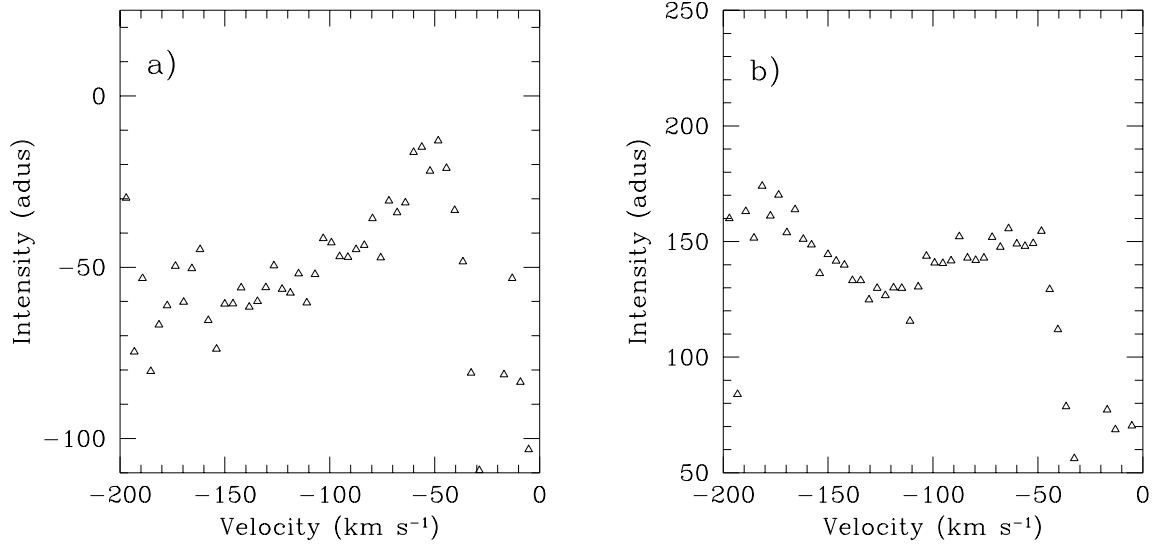


Fig. 11.— H $\alpha$  from the M I cloud: a) 7a - 11a. b) 7a - 4a (both are 900s exposures).

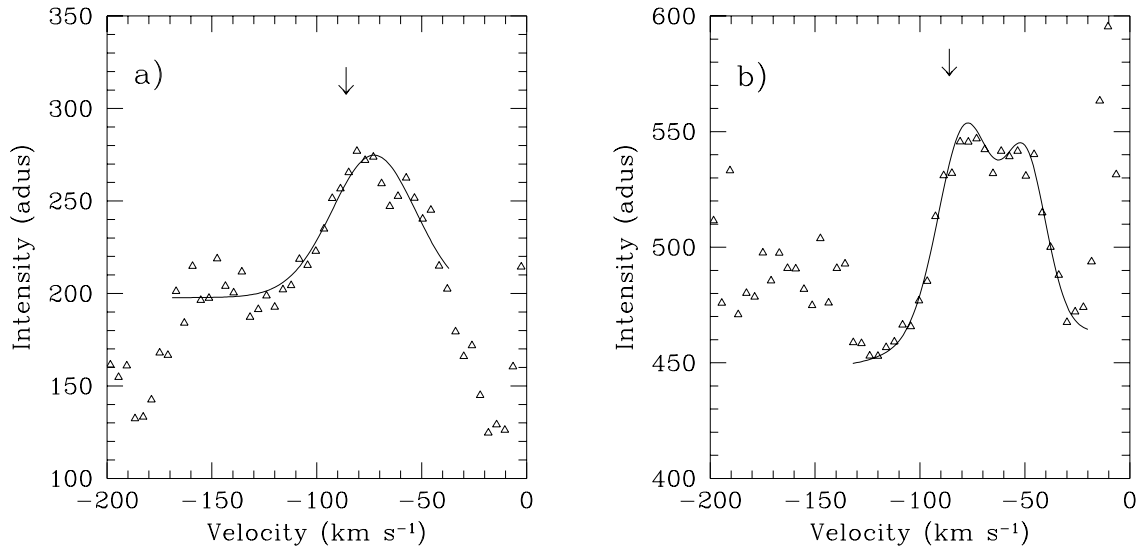


Fig. 12.— H $\alpha$  from the M II cloud: a) 2b - 3b. b) 2b - 4a (both are 900s exposures). The arrows show the velocity of the 21 cm HVC detections.

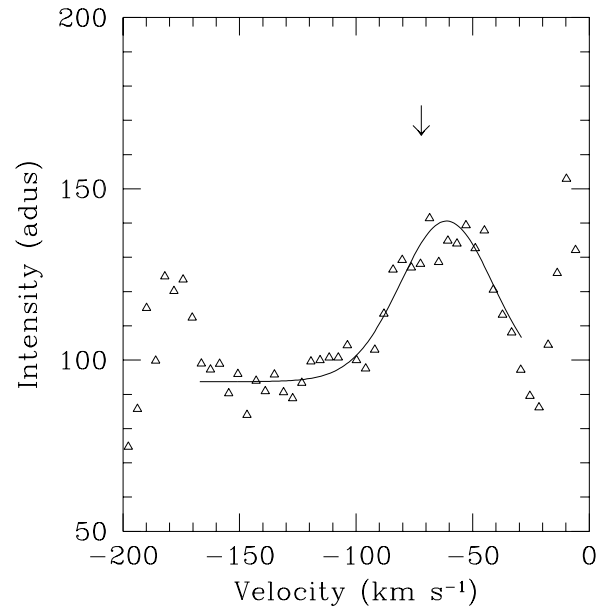


Fig. 13.— H $\alpha$  from the M II cloud: 1b - 4a (900s exposure).

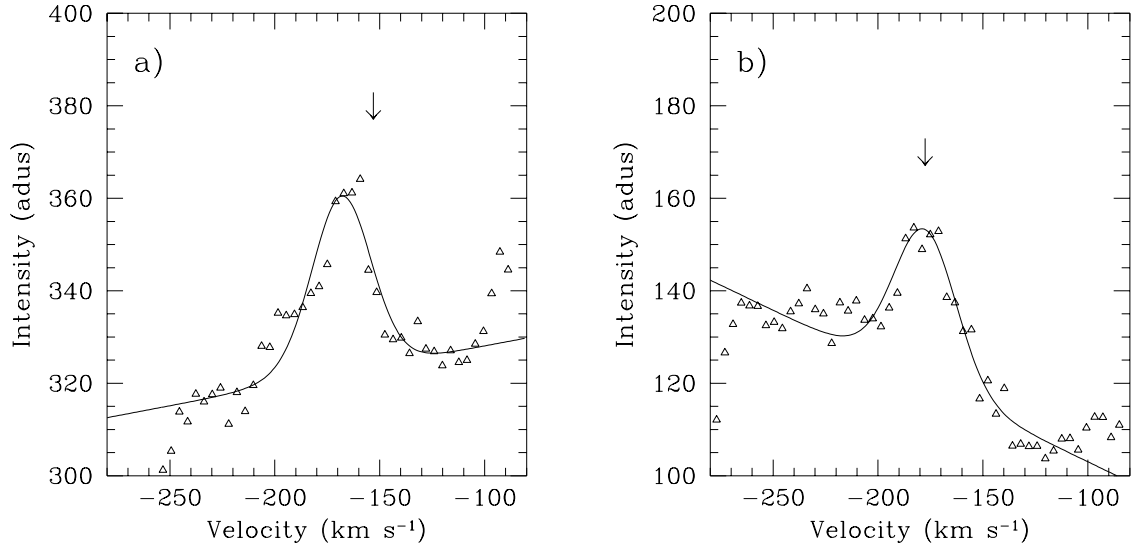


Fig. 14.— H $\alpha$  from the A Complex. a) A III cloud. b) A IV cloud (both normalized to 900s exposure).

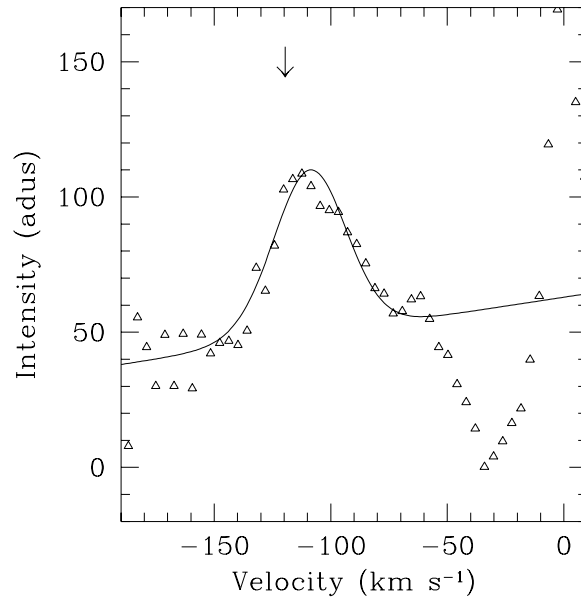


Fig. 15.— H $\alpha$  from the C cloud (normalized to 900s exposure).

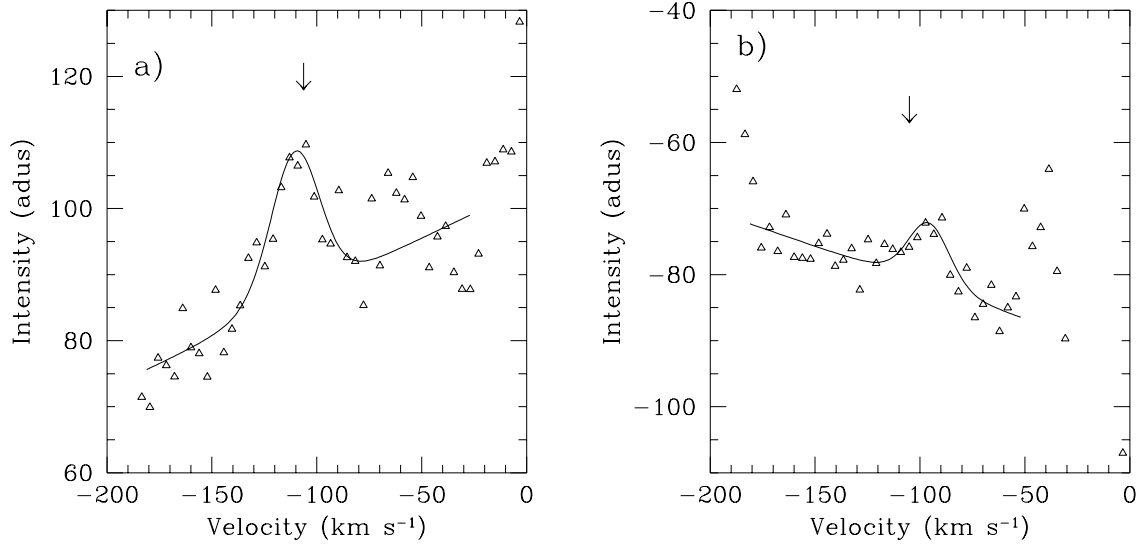


Fig. 16.— [S II] from the M I cloud: a) 1a - 4a. b) 6a - 12a (both normalized to 900s exposure). The arrows show the velocity of the associated H $\alpha$  emission lines.

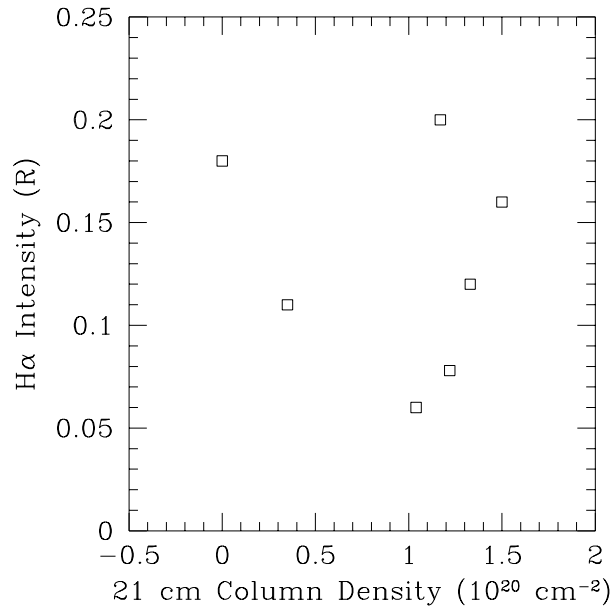


Fig. 17.— H $\alpha$  intensity versus 21 cm column density for the M Complex

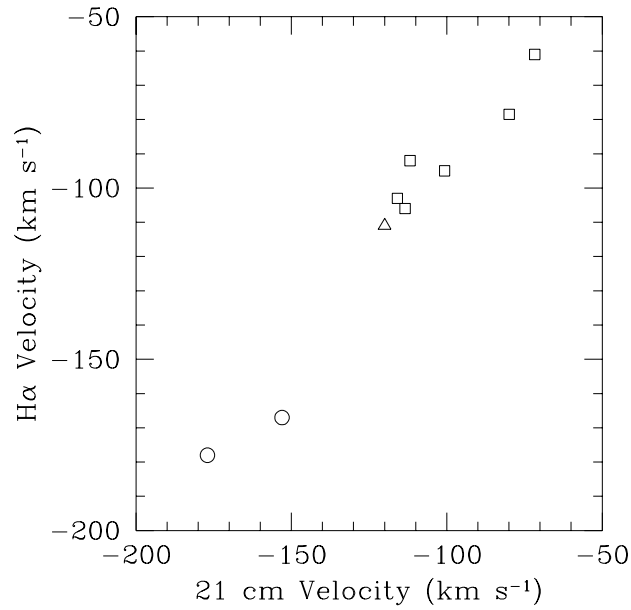


Fig. 18.— H $\alpha$  velocity versus 21 cm velocity. Squares: M Complex, Circles: A Complex, Triangle: C Complex